

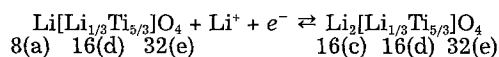
Zero-Strain Insertion Material of $\text{Li}[\text{Li}_{1/3}\text{Ti}_{5/3}]\text{O}_4$ for Rechargeable Lithium Cells

Tsutomu Ohzuku,* Atsushi Ueda,** and Norihiro Yamamoto

Electrochemistry and Inorganic Chemistry Laboratory, Department of Applied Chemistry, Faculty of Engineering, Osaka City University, Sugimoto 3-3-138, Sumiyoshi, Osaka 558, Japan

ABSTRACT

$\text{Li}[\text{Li}_{1/3}\text{Ti}_{5/3}]\text{O}_4$ having a defect spinel-framework structure ($\text{Fd}\bar{3}m$; $a = 8.36 \text{ \AA}$) was prepared and examined in non-aqueous lithium cells. $\text{Li}[\text{Li}_{1/3}\text{Ti}_{5/3}]\text{O}_4$ (white in color) was reduced to $\text{Li}_2[\text{Li}_{1/3}\text{Ti}_{5/3}]\text{O}_4$ (dark blue) at a voltage of 1.55 V and the reaction was highly reversible. X-ray diffraction measurements indicated that the lattice dimension did not change during the reaction



Since the reaction consists of lithium ion and electron insertion into/extraction from the solid matrix without a noticeable change in lattice dimension, called a zero-strain insertion reaction, capacity failure due to the damage to the solid matrix was not observed even after 100 cycles. Feasibility of zero-strain insertion materials for advanced batteries is discussed based on the experimental results.

Introduction

Electrochemical reactions consisting of electron and lithium ion insertion into/extraction from a solid matrix without the destruction of the core structure are called topotactic reactions and the materials for which such reversible reactions proceed are called insertion materials.¹ The reversible characteristics of insertion materials can be used for both positive and negative electrodes for advanced lithium batteries, called lithium ion (shuttlecock) cells or rocking chair cells, in which lithium ions shuttle between two insertion materials.^{2,3} Electrochemical charge and discharge of insertion materials are normally accompanied by a change in lattice dimensions,¹ which results in the physical movements of the positive and negative electrode, together with separator, back and forth during charge and discharge. Capacity failure of these cells may be primarily derived from the change in lattice dimensions as the materials cycle between their two states.¹ Therefore, zero-strain insertion materials, whose lattice dimensions do not change, are ideal for long-life rechargeable batteries.

We report here a zero-strain insertion material, $\text{Li}[\text{Li}_{1/3}\text{Ti}_{5/3}]\text{O}_4$, by showing the x-ray diffraction measurements for $\text{Li}_{1+x}[\text{Li}_{1/3}\text{Ti}_{5/3}]\text{O}_4$ ($0 \leq x < 1$) together with its electrochemical discharge and charge.

Experimental

The Li-Ti-O ternary phases were prepared by heating a mixture of TiO_2 (anatase; Wako Pure Chemical Ind. Ltd., Japan) and $\text{LiOH} \cdot \text{H}_2\text{O}$ at 800°C for 12 h under a nitrogen stream.⁴⁻⁷ Atomic ratios of Li/Ti were varied from 0 to 2. The reaction product was ground and then stored in a desiccator under blue silica gel. The samples were characterized by x-ray diffraction (XRD). XRD data were obtained by using an x-ray diffractometer (Type XD-3A, Shimadzu Corp., Japan) with Cu- K_α radiation, equipped with a diffracted beam graphite monochromator. The electrochemical cells and the data acquisition systems used in this study are the same as described in a previous paper.⁸ Preliminary

electrochemical tests were done using pellets of prepared samples (11 mm diam and ca. 0.5 mm thick). These cathode pellets (0.08 g) were made by pressing the samples without the addition of any conductive binder. The cells were discharged to 1.2 V and then charged to 3.5 V at a rate of $0.3 \text{ mA} \cdot \text{cm}^{-2}$ ($3.8 \text{ mA} \cdot \text{g}^{-1}$) at 30°C . The current was arbitrarily chosen in order to obtain nearly steady voltage-time curves with accessible rechargeable capacities. The discharge-charge cycles were performed until nearly steady rechargeable capacity was obtained.

For extended cycle tests and XRD studies of $\text{Li}_4\text{Ti}_5\text{O}_{12}$ which was selected from the preliminary electrochemical tests, acetylene black and Teflon were used in preparing cathodes. The composition of the cathode mix was 88 weight percent (w/o) $\text{Li}_4\text{Ti}_5\text{O}_{12}$, 6 w/o acetylene black, and 6 w/o Teflon binder (T-30J, Du Pont-Mitsui Fluorochemicals Co., Ltd., Japan). The prepared cathodes ($15 \times 20 \text{ mm}$) were dried under vacuum at about 150°C for 15 h. The current applied was $0.17 \text{ mA} \cdot \text{cm}^{-2}$ for both extended cycle tests and XRD studies to obtain data with one-to-one correspondence between structural and electrochemical information.⁸ Lithium metal was used as an anode. The electrolyte used was 1M LiClO_4 dissolved in ethylene carbonate (EC)/1,2-dimethoxyethane (DME) solution (1:1 by volume). In fabricating the cells, all materials except the electrolyte and lithium metal were dried under vacuum at about 60°C for at least 2 h before fabrication to avoid possible contamination with water. All procedures for handling and fabricating the cells were performed in an argon-filled glove box. Other experimental conditions are given in the Results and Discussion section.

Results and Discussion

Preparation and characterization of Li-Ti-O ternary phases.—The prepared samples of Li-Ti-O ternary phases were white in color indicating that all samples were electronic insulators. Figure 1 shows the initial discharge capacities together with their rechargeable capacities for the samples as a function of the atomic ratio Li/Ti in the samples. A conductive binder, such as acetylene black or graphite, was not used in the experiments to examine intrinsic electrochemical behavior of the samples. As shown

* Electrochemical Society Active Member.

** Electrochemical Society Student Member.

in Fig. 1, the maximum rechargeable capacity was obtained at $\text{Li}/\text{Ti} = 4/5$ which was a breakpoint in the initial discharge capacities *vs.* Li/Ti plots. In the region $1/2 < \text{Li}/\text{Ti} \leq 4/5$ the initial discharge capacities are constant at about $160 \text{ mAh} \cdot \text{g}^{-1}$ while the rechargeable capacities increase as the Li/Ti ratio increases. In the region $4/5 < \text{Li}/\text{Ti} < 2$ both initial discharge and rechargeable capacities decrease almost linearly as the Li/Ti ratio increases. Since the atomic ratio Li/Ti at the breakpoint is $4/5$, the chemical composition is estimated to be $2\text{Li}_2\text{O} \cdot 5\text{TiO}_2$ based on Li_2O and TiO_2 (both are white in color) or $\text{Li}_4\text{Ti}_5\text{O}_{12}$.

In order to examine whether or not a single phase exists at $\text{Li}/\text{Ti} = 4/5$, XRD examinations were carried out. Results are shown in Fig. 2. The XRD pattern in Fig. 2 (a) is identified as Li_2TiO_3 ($\text{Li}/\text{Ti} = 2$). The Miller indexes are given for a monoclinic lattice ($a = 5.064 \text{ \AA}$, $b = 8.783 \text{ \AA}$, $c = 9.731 \text{ \AA}$, and $\beta = 100.0^\circ$). The XRD pattern in Fig. 2 (e) is of anatase TiO_2 ($\text{Li}/\text{Ti} = 0$) having a tetragonal lattice with $a = 3.792 \text{ \AA}$ and $c = 9.514 \text{ \AA}$. At $\text{Li}/\text{Ti} = 4/5$ the XRD pattern which is different from either Li_2TiO_3 ($\text{Li}/\text{Ti} = 2$) and anatase TiO_2 ($\text{Li}/\text{Ti} = 0$) is obtained. All these diffraction lines are indexed by assuming a cubic lattice as is discussed later. As can be seen in Fig. 2, a mixture of anatase TiO_2 and $\text{Li}_4\text{Ti}_5\text{O}_{12}$ is obtained for $0 < \text{Li}/\text{Ti} < 4/5$, and a mixture of $\text{Li}_4\text{Ti}_5\text{O}_{12}$ and Li_2TiO_3 is obtained for $4/5 < \text{Li}/\text{Ti} < 2$. At $\text{Li}/\text{Ti} = 4/5$ the XRD pattern of a single phase is obtained.

Crystal structure of $\text{Li}_4\text{Ti}_5\text{O}_{12}$.—In analyzing the XRD data a defect spinel-framework structure was assumed⁴⁻⁷ and all diffraction lines were indexed in terms of (h, k, l) for a face-centered cubic lattice. The lattice parameter a was obtained to be $a = 8.365 \text{ \AA}$ by a least squares method using 14 diffraction lines. In calculating the intensities we assume a space group $\text{Fd}\bar{3}\text{m}$ in which lithium ions are located at the tetrahedral 8(a) sites (or half of the octahedral 16(c)

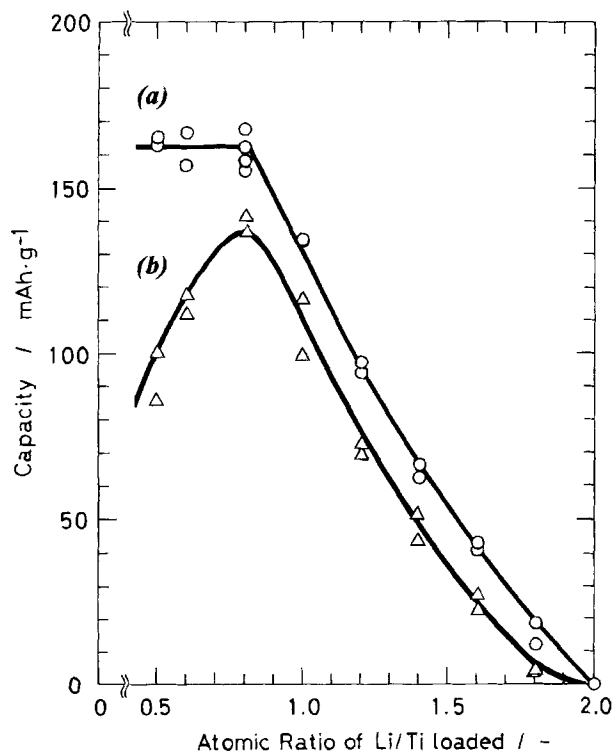


Fig. 1. Electrochemical characterization of white samples (Li-Ti-O ternary phases) in terms of (a) initial discharge capacity and (b) rechargeable capacity as a function of atomic ratio Li/Ti loaded in preparing samples. Conductive binder was not used in order to obtain intrinsic electrochemical characters of the samples. Compressed pellets (11 mm diam and ca. 0.5 mm thick) were used as cathodes in nonaqueous lithium cells. Electrochemical tests were done at a rate of $0.3 \text{ mA} \cdot \text{cm}^{-2}$ ($3.8 \text{ mA} \cdot \text{g}^{-1}$) at 30°C .

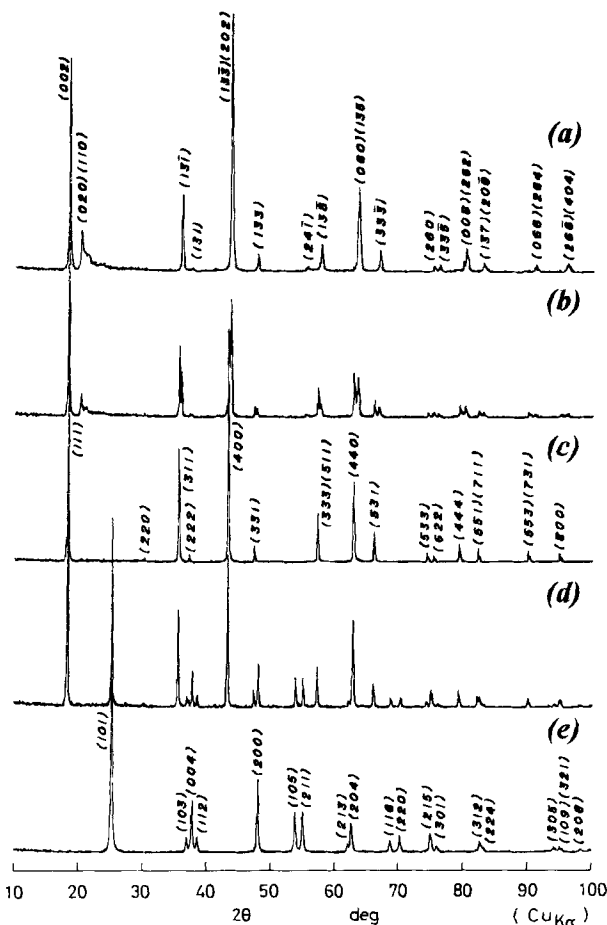


Fig. 2. X-ray diffraction patterns of white samples (Li-Ti-O ternary phases) prepared from anatase TiO_2 and LiOH by atomic ratio Li/Ti ; (a) 2, (b) $7/5$, (c) $4/5$, (d) $1/2$, and (e) 0. XRD pattern (a) is identified as Li_2TiO_3 (monoclinic; $a = 5.064 \text{ \AA}$, $b = 8.783 \text{ \AA}$, $c = 9.731 \text{ \AA}$, and $\beta = 100.0^\circ$) and pattern (e) is identified as anatase TiO_2 (tetragonal; $a = 3.792 \text{ \AA}$ and $c = 9.514 \text{ \AA}$). Miller indexes in (c) are given by assuming a cubic lattice ($a = 8.365 \text{ \AA}$).

sites), and tetravalent titanium ions ($3d^0$) and lithium ions are randomly distributed at octahedral 16(d) sites by the ratio $\text{Li}/\text{Ti} = 1/5$, while oxygen ions are located at the 32(e)

Table I. Structural analysis of $\text{Li}_{4/3}\text{Ti}_{5/3}\text{O}_4$. Unit cell parameter was determined to be $a = 8.365 \text{ \AA}$ by assuming a cubic lattice by the least squares method using 14 diffraction lines.

| No. | (h, k, l) | $d_{\text{obs}}/\text{\AA}$ | $d_{\text{cal}}/\text{\AA}$ | I_{obs} | I_{cal}^{*1} | I_{cal}^{*2} |
|-----|-----------|-----------------------------|-----------------------------|------------------|-----------------------|-----------------------|
| 1 | (1, 1, 1) | 4.849 | 4.830 | 100.00 | 98.51 | 100.71 |
| 2 | (3, 1, 1) | 2.527 | 2.522 | 42.04 | 39.77 | 28.43 |
| 3 | (4, 0, 0) | 2.092 | 2.091 | 64.97 | 59.34 | 70.99 |
| 4 | (3, 3, 1) | 1.920 | 1.919 | 5.88 | 5.18 | 6.18 |
| 5 | (3, 3, 3) | 1.611 | 1.610 | 19.12 | 0.79 | 0.43 |
| 6 | (5, 1, 1) | 1.611 | 1.610 | 19.12 | 19.18 | 14.66 |
| 7 | (4, 4, 0) | 1.479 | 1.479 | 32.65 | 33.28 | 34.07 |
| 8 | (5, 3, 1) | 1.414 | 1.414 | 10.44 | 12.94 | 13.59 |
| 9 | (5, 3, 3) | 1.275 | 1.276 | 3.70 | 4.66 | 3.28 |
| 10 | (6, 2, 2) | 1.261 | 1.261 | 2.82 | 3.77 | 4.76 |
| 11 | (4, 4, 4) | 1.207 | 1.207 | 7.21 | 7.27 | 9.08 |
| 12 | (5, 5, 1) | 1.171 | 1.171 | 5.10 | 5.35 | 5.43 |
| 13 | (7, 1, 1) | 1.171 | 1.171 | 5.10 | 1.01 | 1.19 |
| 14 | (5, 5, 3) | 1.089 | 1.089 | 4.95 | 4.49 | 3.43 |
| 15 | (7, 3, 1) | 1.089 | 1.089 | 4.95 | 2.25 | 1.38 |
| 16 | (8, 0, 0) | 1.045 | 1.046 | 3.73 | 4.83 | 5.00 |

Calculations were made by assuming a space group $\text{Fd}\bar{3}\text{m}$ in which Li^+ ions were located at (*1) tetrahedral 8(a) sites or (*2) half of octahedral 16(c) sites, Li^+ and Ti^{4+} ions were randomly distributed at octahedral 16(d) sites by the ratio $\text{Li}/\text{Ti} = 1/5$, and O^{2-} ions were located at 32(e) sites with oxygen positional parameter (*1) 0.262 ($R = 0.067$) or (*2) 0.264 ($R = 0.120$).

sites with the oxygen positional parameter, u . The results are shown in Table I. The R value was calculated from $\sum/I_{\text{ob}} - I_{\text{cal}}/\sum I_{\text{ob}}$. We analyzed the XRD data based on two structural models, *i.e.*, $\text{Li}^{8(a)}[\text{Li}_{1/3}\text{Ti}_{5/3}]^{16(d)}\text{O}_4^{32(e)}$ and $\text{Li}^{16(c)}[\text{Li}_{1/3}\text{Ti}_{5/3}]^{16(d)}\text{O}_4^{32(e)}$, in which superscripts indicate the number of equivalent sites combined with Wyckoff letters for the space group $\text{Fd}\bar{3}\text{m}$. The determination of the locations of lithium ions in transition metal oxides is usually very difficult to determine by XRD alone because the atomic scattering factor of lithium ion (f_{Li^+}) is very small, *i.e.*, $f_{\text{Li}^+} = 2.0$ at $\sin \theta/\lambda = 0$. However, the locations of the lithium ions at the tetrahedral 8(a) sites or octahedral 16(c) sites reflect upon the XRD intensities in this structure, especially for the (3, 1, 1) and (4, 0, 0) lines, as shown in Table I. The R value is remarkably decreased when we assume the lithium ions are at the tetrahedral 8(a) sites ($R = 0.067$) compared to 1/2 occupation at the octahedral 16(c) sites ($R = 0.120$) while both structural models give almost the same oxygen positional parameter $u = 0.264 - 0.265$. This suggests that $\text{Li}^{8(a)}[\text{Li}_{1/3}\text{Ti}_{5/3}]^{16(d)}\text{O}_4^{32(e)}$ is the probable structure, because the smaller R -value means the better fitness between the observed and calculated intensities as seen in Table I. Observation of the weak (2, 2, 0) diffraction line in Fig. 2 (c) also supports this formulation. The oxygen positional parameter $u = 0.265$ and the structural formulation are in good agreement with those reported by Johnston⁵ ($u = 0.262$ for $\text{Li}_{4/3}\text{Ti}_{5/3}\text{O}_4$) while their cubic lattice parameter $a = 8.357 \text{ \AA}$ is smaller than our value. Murphy *et al.*⁹ report $a = 8.357 \text{ \AA}$, and Harrison *et al.*⁶ also report $a = 8.358 \text{ \AA}$. These values are consistent with that by Johnston.⁵ Colbow *et al.*⁷ report $a = 8.367 \text{ \AA}$ which is in good agreement with our value $a = 8.365 \text{ \AA}$. About 0.01 \AA difference between the two groups can be seen in the lattice parameters. According to the relationship between the lattice parameter a and y in $\text{Li}_{1+y}\text{Ti}_{2-y}\text{O}_4$ given by Johnston,⁵ our value of $a = 8.365 \text{ \AA}$ corresponds to $y = 0.275$ at which the sample contains trivalent titanium ions and is blue or blue black in color (electronic conductor). However, our sample ($a = 8.365 \text{ \AA}$) and that by Colbow *et al.*⁷ ($a = 8.367 \text{ \AA}$) are white in color (electronic insulator). Additional defects such as cation vacancies may be involved in our sample, leading to about 0.01 \AA lattice dilution, although we cannot specify it by XRD alone.

As described above, we characterized the sample having a defect spinel-framework structure $\text{Li}^{8(a)}[\text{Li}_{1/3}\text{Ti}_{5/3}]^{16(d)}\text{O}_4^{32(e)}$ ($\text{Fd}\bar{3}\text{m}$; $a = 8.365 \text{ \AA}$, oxygen positional parameter $u = 0.265$).

Electrochemical discharge and charge.— $\text{Li}[\text{Li}_{1/3}\text{Ti}_{5/3}]\text{O}_4$ is already known to be electroactive in nonaqueous lithium cells.^{7,9} Figure 3 shows continuous discharge and subsequent charge curves for a $\text{Li}/\text{Li}[\text{Li}_{1/3}\text{Ti}_{5/3}]\text{O}_4$ cell at a rate of $0.17 \text{ mA} \cdot \text{cm}^{-2}$ ($5 \text{ mA} \cdot \text{g}^{-1}$) at 30°C . In examining the cyclability of $\text{Li}[\text{Li}_{1/3}\text{Ti}_{5/3}]\text{O}_4$, acetylene black and Teflon binder were used to prepare the cathode in order to give electrical contact to every particle and also to supply electrolyte inside the cathode. The initial open-circuit voltage was 2.95–3.00 V. During the discharge the voltage drops quickly down to below 2 V and decreases as the reaction proceeds until the voltage reaches about 1.55 V (initial 5% of discharge capacity), after which the voltage is almost independent of the degree of reduction. During the final 5% of discharge the voltage drops below 1.55 V and then falls sharply. When the discharged cell is charged, the voltage follows just above the discharge voltages in the reverse direction. The cells were cycled between 1.2 and 3.5 V. In Fig. 3 selected charge-discharge curves obtained during a 100 cycle test are shown. One cell exhibits $160 \text{ mA} \cdot \text{g}^{-1}$ of rechargeable capacity. Three curves for the 4th, 20th, and 40th cycle are shown. The other shows $150 \text{ mA} \cdot \text{g}^{-1}$ of rechargeable capacity. Three curves for the 60th, 80th, and 100th cycle are shown. The reason for the difference in rechargeable capacities between the two groups is derived from XRD examination followed by the refabrication of the cell after the 50th cycle as is shown

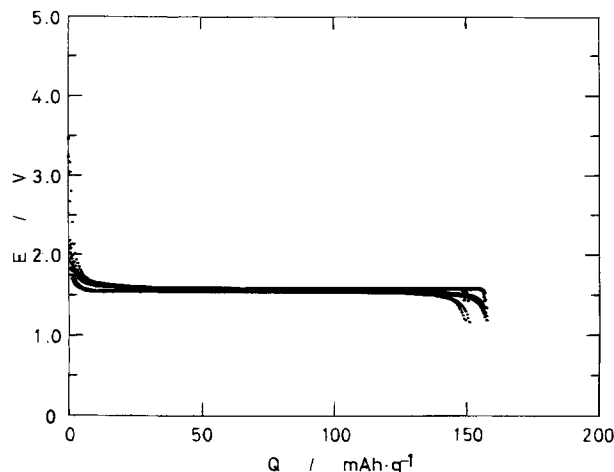
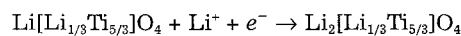


Fig. 3. Discharge and charge curves of two $\text{Li}/\text{Li}[\text{Li}_{1/3}\text{Ti}_{5/3}]\text{O}_4$ cells at a rate of $0.17 \text{ mA} \cdot \text{cm}^{-2}$ ($5 \text{ mA} \cdot \text{g}^{-1}$) at 30°C . The electrolyte used was 1 M LiClO_4 dissolved in EC/DME (1:1 by volume). Cathode mix consists of 88 w/o $\text{Li}[\text{Li}_{1/3}\text{Ti}_{5/3}]\text{O}_4$, 6 w/o acetylene black, and 6 w/o Teflon binder. The one cell exhibiting $160 \text{ mA} \cdot \text{g}^{-1}$ of rechargeable capacity consists of three curves for the 4th, 20th, and 40th cycle, and the other showing $150 \text{ mA} \cdot \text{g}^{-1}$ of rechargeable capacity consists of three curves for the 60th, 80th, and 100th cycle. Difference in rechargeable capacity is derived from XRD examination followed by the refabrication of the cell after the 50th cycle as shown in Fig. 6 and 7.

below. The value of x in $\text{Li}_{1+x}[\text{Li}_{1/3}\text{Ti}_{5/3}]\text{O}_4$ is calculated from the discharge (and charge) capacity and the theoretical capacity of $175 \text{ mA} \cdot \text{g}^{-1}$ based on the sample weight by assuming 100% efficiency for the reaction



As can be seen in Fig. 3, the rechargeable capacity is $150\text{--}160 \text{ mA} \cdot \text{g}^{-1}$, which does not fade rapidly upon cycling. The characteristic features of the voltage profile are (i) the extremely flat operating voltage at about 1.55 V and (ii) the very close operating voltages during charge and discharge. Feature (i) suggests a two-phase reaction proceeds over almost the entire range. However, two-phase reactions for insertion materials having three-dimensional framework structures, such as $\text{RuO}_2\text{--LiRuO}_2$ ¹⁰ and $\text{LiMn}_2\text{O}_4\text{--Li}_2\text{Mn}_2\text{O}_7$,¹¹ normally show a hysteresis in their charge and discharge curves even for open-circuit voltages,¹⁰ and their rechargeable capacities fade quickly on cycling. Such characteristics are not seen in Fig. 3. Of these, a most important characteristic of this material is the lack of capacity fading during the charge-discharge cycles.

X-ray diffraction measurements.—In order to examine whether the electrochemical reaction of $\text{Li}_{1+x}[\text{Li}_{1/3}\text{Ti}_{5/3}]\text{O}_4$ proceeds in a homogeneous phase or two phases, x-ray diffraction examinations were carried out *ex situ*. Figure 4 shows the discharge/charge curves for samples prepared for XRD study. The arrows directed upward indicate the compositions at which XRD examinations were done during the reduction of $\text{Li}[\text{Li}_{1/3}\text{Ti}_{5/3}]\text{O}_4$, and arrows directed downward for the oxidation of the reduction product. The samples were covered with a polyethylene film while obtaining the XRD data to prevent the oxidation of the samples by moist air. Five diffraction patterns are shown in Fig. 5. The XRD pattern of $\text{Li}[\text{Li}_{1/3}\text{Ti}_{5/3}]\text{O}_4$ on the top in Fig. 5 was taken from a powdered sample using an aluminum holder and was used for the structural analysis in Table I. We expected XRD patterns which showed the coexistence of cubic and tetragonal phases by analogy of the

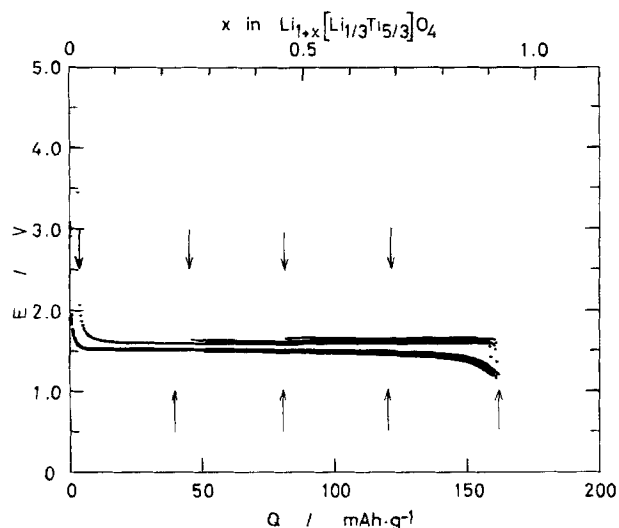


Fig. 4. Records on the preparation of $\text{Li}_{1+x}[\text{Li}_{1/3}\text{Ti}_{5/3}]\text{O}_4$ for XRD examinations. Arrows directed upward indicate the locations at which XRD examinations were done for the reduction of $\text{Li}[\text{Li}_{1/3}\text{Ti}_{5/3}]\text{O}_4$, and arrows directed downward for the oxidation of the samples following $160 \text{ mAh} \cdot \text{g}^{-1}$ of reduction.

results on $\text{LiMn}_2\text{O}_4(\text{Fd}\bar{3}\text{m})/\text{Li}_2\text{Mn}_2\text{O}_4(\text{I}4_1/\text{amd})^{11}$ because both Mn^{3+} and Ti^{3+} are Jahn-Teller ions when electrons are localized. However, the expected change in the locations of

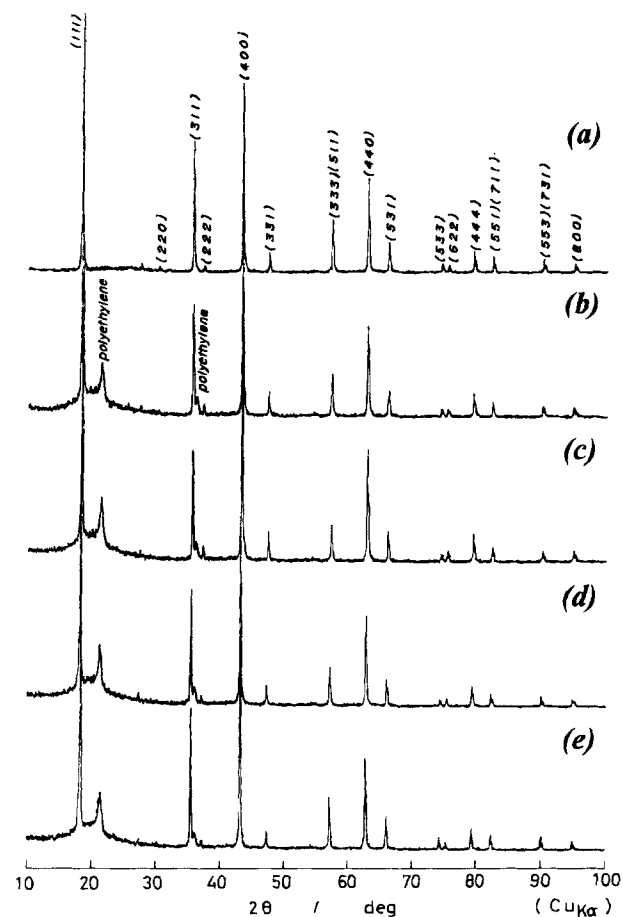
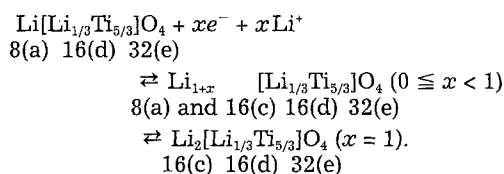


Fig. 5. XRD patterns of $\text{Li}_{1+x}[\text{Li}_{1/3}\text{Ti}_{5/3}]\text{O}_4$; (a) $x = 0$, (b) $x = 0.46$, (c) $x = 0.91$, (d) $x = 0.46$, and (e) $x = 0$. XRD samples were prepared by (a) $0 \text{ mAh} \cdot \text{g}^{-1}$, (b) $80 \text{ mAh} \cdot \text{g}^{-1}$, and (c) $160 \text{ mAh} \cdot \text{g}^{-1}$ of reduction of $\text{Li}[\text{Li}_{1/3}\text{Ti}_{5/3}]\text{O}_4$, and by (d) $80 \text{ mAh} \cdot \text{g}^{-1}$ and (e) $160 \text{ mAh} \cdot \text{g}^{-1}$ of oxidation following $160 \text{ mAh} \cdot \text{g}^{-1}$ of reduction. Capacity in $\text{mAh} \cdot \text{g}^{-1}$ is based on $\text{Li}[\text{Li}_{1/3}\text{Ti}_{5/3}]\text{O}_4$ sample weight.

diffraction lines (Bragg angles) and also line shapes cannot be seen in Fig. 5. The lattice constants observed for 9 samples having different degrees of reduction ranging from $x = 0$ to $x = 0.91$ in $\text{Li}_{1+x}[\text{Li}_{1/3}\text{Ti}_{5/3}]\text{O}_4$ are the same within experimental error, i.e., $a = 8.370 \pm 0.005 \text{ \AA}$. Although the location of the diffraction lines do not change, a change in relative intensities can clearly be seen in Fig. 5. During the reduction of $\text{Li}[\text{Li}_{1/3}\text{Ti}_{5/3}]\text{O}_4$ the intensity of the (5, 3, 3) line becomes weak and that of the (6, 2, 2) line becomes strong, so that the intensity ratio of $I_{(6,2,2)}/I_{(5,3,3)}$ changes from a value above unity to below unity. The unity value occurs at the midpoint of the reaction ($80 \text{ mAh} \cdot \text{g}^{-1}$ of reduction in Fig. 5). Oxidation of $\text{Li}_{1.9}[\text{Li}_{1/3}\text{Ti}_{5/3}]\text{O}_4$ gives identical data with that observed for the reduction of $\text{Li}[\text{Li}_{1/3}\text{Ti}_{5/3}]\text{O}_4$. Such changes in intensity can be explained by assuming that the inserted lithium ions together with the same number of residual lithium ions (originally located at tetrahedral 8(a) sites) begin to occupy the octahedral 16(c) sites, and finally all octahedral 16(c) sites are occupied by lithium ions.

From these electrochemical and XRD results, we formulate the topotactic reaction as



It should be noted that the reduction product $\text{Li}_2[\text{Li}_{1/3}\text{Ti}_{5/3}]\text{O}_4$ still has tetravalent titanium ions (40% of all titanium ions) to accept electrons, but no vacant octahedral sites to accommodate lithium ions. Accordingly, the capacity of $\text{Li}[\text{Li}_{1/3}\text{Ti}_{5/3}]\text{O}_4$ is limited by the number of available octahedral sites to accommodate lithium ions (called lithium ion site-limited capacity).³

We examined the electrochemical and XRD results with respect to both a single-phase reaction and a two-phase reaction. However, both models equally explain the experimental results, so a definitive description of the reaction mechanism cannot be given at this time.

Significance of zero-strain insertion material for advanced batteries.—Since the lattice dimensions do not change during charge and discharge, capacity failure due to electrode crumbling and particle fracture primarily derived from dimensional changes in a unit cell is eliminated. In order to show a significant effect of a zero-strain insertion scheme upon the capacity retention, cycle tests of the $\text{Li}/\text{Li}[\text{Li}_{1/3}\text{Ti}_{5/3}]\text{O}_4$ cells were performed. The results are shown in Fig. 6. Charge and discharge coulombic efficiencies are very close to 100%. Capacity fading due to damage of the solid matrix is hardly observed. In order to confirm whether or not the $\text{Li}[\text{Li}_{1/3}\text{Ti}_{5/3}]\text{O}_4$ matrix was damaged by cycling, XRD examinations of the electrodes after 50 and 100 charge-discharge cycles were carried out. After the 50th and 100th cycle the cell was opened and the positive electrode was taken out of the cell in an argon-filled glove box. The electrode ($15 \times 20 \text{ mm}$) was covered with a polyethylene film, heat-sealed, and then transferred to the x-ray system outside the glove box. After an XRD examination (took about 90 min), the polyethylene film was removed in a glove box and the cell was refabricated by introducing a new lithium electrode and new electrolyte, and then cycle tests were continued. A discontinuous drop in the rechargeable capacity after the 50th cycle is due to the difference in sample history described above. As can be seen in Fig. 7, noticeable changes in the XRD profiles are not observed even after 100 cycles.

In this paper we used an organic electrolyte to examine the electrochemical properties. However, the electrolyte need not be based on organic solvents. Lithium ion conductive solid electrolytes may be a possible replacement for a liquid electrolyte. Making solid electrolytes for lithium ion

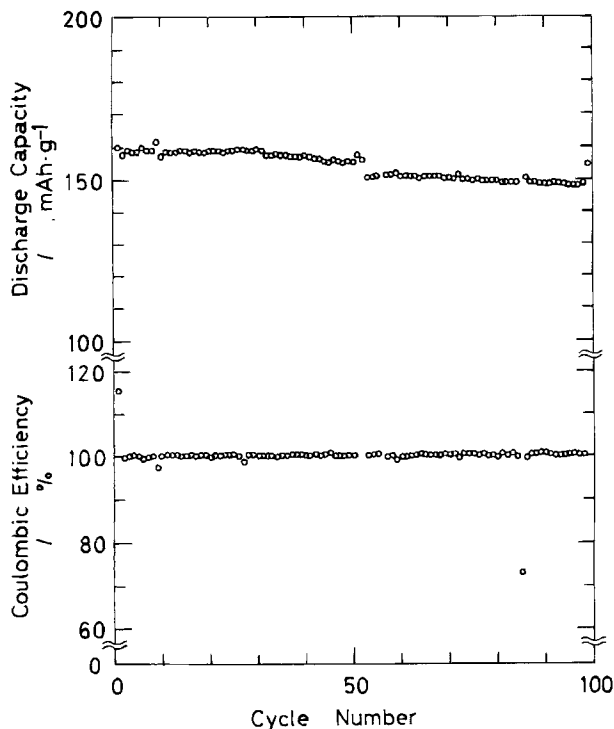


Fig. 6. Discharge capacities and charge-discharge coulombic efficiencies of a Li/Li[Li_{1/3}Ti_{5/3}]O₄ cell as a function of cycle number. The cell was cycled between 1.2 and 3.5 V. After 50th cycle XRD examination was carried out and the cell was refabricated with introducing a fresh lithium electrode and electrolyte. During a couple of cycles for a renewed cell, rechargeable capacities were leveled off at about 150 mAh · g⁻¹. Charge-discharge coulombic efficiencies were very close to 100% except for accidents which occurred at the 1st, 51st, 52nd, and 85th cycle.

(shuttlecock) batteries is normally very hard because of the difficulty of avoiding breaks, especially at the insertion material/solid electrolyte interfaces. These fractures are induced by stress derived from changes in lattice dimensions of the insertion materials during charge and discharge. The zero-strain insertion material described here makes it possible to use lithium ion conductive solid electrolytes in lithium ion batteries. We believe that zero-strain insertion materials and a lithium ion conductive solid electrolyte (ceramics) are necessary for the implementation of long-life, high-volume, and safe solid-state lithium ion batteries. In order to establish the materials science for long-life lithium ion batteries further understanding of the zero-strain insertion material Li[Li_{1/3}Ti_{5/3}]O₄ is extremely important as is answering the question of the single-phase/two-phase cathode material. Neutron diffraction and the detailed reversible potential measurements will give more insights into a zero-strain insertion mechanism. Such developments are under progress in our laboratory.

Acknowledgments

The authors wish to thank Mr. Takayuki Yanagawa and Mr. Yoshikumi Miyamoto for their help on sample preparation and cycle tests. One of us (T.O.) is indebted to Dr. Taketsugu Hirai, Professor Emeritus from Osaka City University, throughout the research. The present work was partially supported by a Grant-in-Aid for Scientific Research from the Ministry of Education, Science and Culture, Japan.

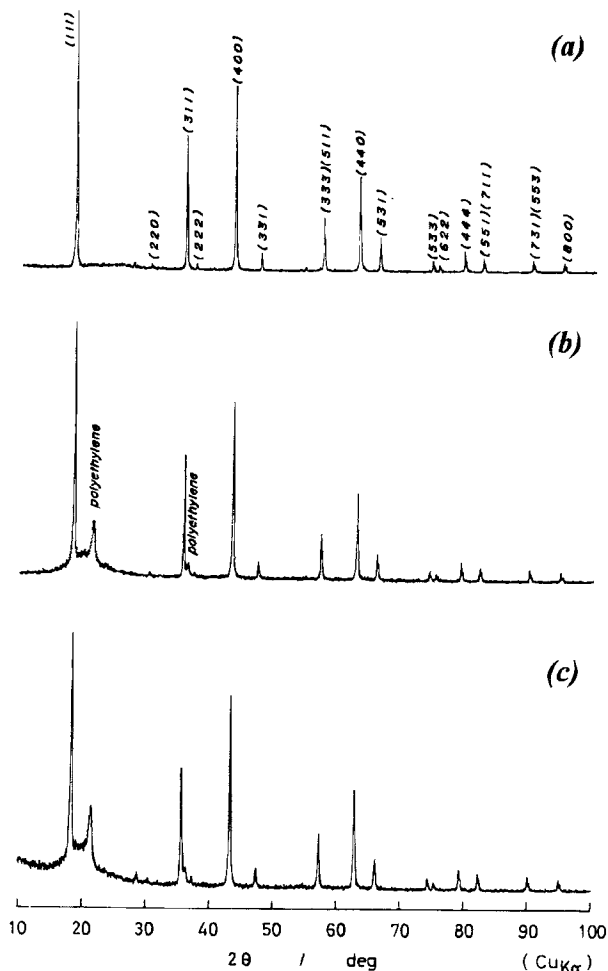


Fig. 7. XRD pattern of Li[Li_{1/3}Ti_{5/3}]O₄ experienced (b) 50 and (c) 100 charge-discharge cycles. Starting material Li[Li_{1/3}Ti_{5/3}]O₄ is also shown in (a) for comparison.

Manuscript submitted Aug. 3, 1994; revised manuscript received Jan. 18, 1995.

Osaka City University assisted in meeting the publication costs of this article.

REFERENCES

1. T. Ohzuku and A. Ueda, *Solid State Ionics*, **69**, 201 (1994) and references therein.
2. B. Scrosati, *This Journal*, **139**, 2776 (1992).
3. T. Ohzuku, in *Lithium Batteries. New Materials, Developments and Perspectives*, G. Pistoia, Editor, p. 239, Elsevier, Amsterdam (1994).
4. G. Blasse, *Philips Res. Repts. Suppl.*, **3**, 125 (1964).
5. D. C. Johnston, *J. Low Temp. Phys.*, **25**, 145 (1976).
6. M. R. Harrison, P. P. Edwards, and J. B. Goodenough, *Philos. Mag.*, **52**, 679 (1985).
7. K. M. Colbow, J. R. Dahn, and R. R. Haering, *J. Power Sources*, **26**, 397 (1989).
8. T. Ohzuku, A. Ueda, and M. Nagayama, *This Journal*, **140**, 1862 (1993).
9. D. W. Murphy, R. J. Cava, S. M. Zahurak, and A. Santoro, *Solid State Ionics*, **9&10**, 413 (1983).
10. T. Ohzuku, K. Sawai, and T. Hirai, *This Journal*, **137**, 3004 (1990).
11. T. Ohzuku, M. Kitagawa, and T. Hirai, *ibid.*, **137**, 769 (1990).